Reading Circular Analogue Gauges using Digital Image Processing

Jakob S. Lauridsen[1], Julius A. G. Grassmé[1], Malte Pedersen[1], David Getreuer Jensen[2],
Søren Holm Andersen[2] and Thomas B. Moeslund[1]

[1]*Section of Media Technology, Aalborg University, Denmark*
[2]*EnviDan, Aalborg, Denmark*

Keywords: Computer Vision, Circular Analogue Gauge, Gauge Reading Principal Component Analysis, Expectation Maximization, Digital Time Series, Parametric Object Classification.

Abstract: This paper presents an image processing based pipeline for automated recognition and translation of pointer movement in analogue circular gauges. The proposed method processes an input video frame-wise in a module based manner. Noise is minimized in each image using a bilateral filter before a Gaussian mean adaptive threshold is applied to segment objects. Subsequently, the objects are described by a set of proposed features and classified using probability distributions estimated using Expectation Maximization. The pointer is classified by the Mahalanobis distance and the angle of the pointer is determined using PCA. The output is a low pass filtered digital time series based on the temporal estimations of the pointer angle. Seven test videos have been processed by the algorithm showing promising results. Both source code and video data are publicly available.

1 INTRODUCTION

Analogue pointer-type dials are widely applied in both industrial and personal products where information such as pressure or speed is displayed. This includes old waste water pumping stations, which can have analogue pressure gauges mounted on the pump as the main instrument to inspect the condition of the system. Typically a field operator is responsible for reading and recording the data from the gauge to evaluate the performance of the pump. This is a time consuming and expensive process and it is prone to human errors. An alternative to the manual readings is to record a video of the gauge and analyze the pressure variations using computer vision techniques.
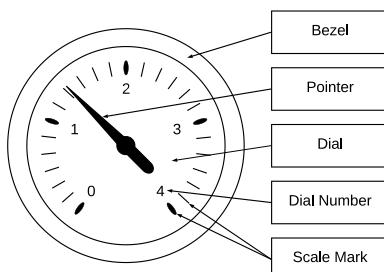

Figure 1: Illustration of a circular pressure gauge with highlighted features and their respective terms.

This paper presents such an approach, that automatically recognizes key parts of analogue circular gauges and identifies the transient behaviour of the pointer over the course of the video in order to create a digital time series. The terminology that will be used throughout the paper when describing gauges is presented in Figure 1.

2 RELATED WORK

One of the early attempts to describe and break down the problem of digitizing analogue dials was presented by Sablatnig et al., who proposed a design strategy for automatically reading dials of various shapes using pattern recognition techniques (Sablatnig and Kropatsch, 1994). Some years later Alegria et al. developed a calibration system capable of reading dials using thresholding, image thinning and the Hough line transform. However, this system was only able to read dials where the pointer moves in a half circle (Alegria and Serra, 2000). The Hough line transform and its variations have since been a popular method for reading the pointer's angle yielding feasible results (Ye et al., 2013) (Jiannan Chi, 2015) (Jiale et al., 2011). Others have used least squares as an alternative yielding more accurate results in general (Yang

et al., 2014) (Wang et al., 2013).

M. Gellaboina uses a rotation of segmented objects and unwinding of the dial to read round pressure gauges (Gellaboina et al., 2013). The unwinding technique is also used by Zheng et al., who furthermore made the system more robust using colour correction and perspective transforms (Zheng et al., 2016). Yi et al. provide an algorithm robust to axial noise changes by not assuming a perfect circular shape, finding the scale marks with the K-means clustering algorithm (Yi et al., 2017).

The aforementioned contributions exclude the association of unit related text on the dial to the scale as a part of the automation. Sun et al. include this in their contribution by recognizing the numbers in the dial and associating these to the dial scale (Sun et al., 2014).

A consistent flaw within the field is the lack of public data, as it has not been possible to locate the source code, videos, images or other relevant material from any of the state-of-the-art methods. Furthermore, several articles lack detailed descriptions of critical parts of the implementations, leading to a serious inadequacy within the field, as it is not possible to make accurate comparisons and benchmark tests.

3 CONTRIBUTION

Based on the shortcomings of the current state-of-the-art methods, the following contributions will be presented in the paper:

- Presentation of a new state-of-the-art method based on parametric classification of the pointer and scale marks.

- Application example: obtaining a digital time series based on a recording of an analogue pressure gauge.

- Source code and video data are published for benchmarking.

4 APPROACH

We propose a system that takes a video of a circular analogue gauge as input and translates the signal into a digital time series.

The overall structure of the module based system is illustrated in Figure 2 and every part will be described in the following sections. It should be noted that there has not been implemented a module for classifying the dial numbers as there exist excellent open source solutions capable of handling this.
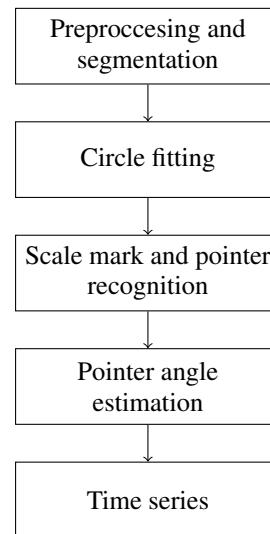
Figure 2: Algorithmic structure of automatic pressure reading system.

4.1 Preprocessing and Segmentation

The need to separate and segment objects with minimal error is a traditional image processing problem. In the given case, the problem can be boiled down to handling minor variations in light, contrast, and blur assuming that the camera is kept relatively steady in front of a well-lit gauge.

This problem has previously been handled using local contrast normalization (Gellaboina et al., 2013), multi-scale retinex to reduce the influence of different brightness levels (Zheng et al., 2016), and a laplacian filter to enhance the sharpness of the image (Selvathai et al., 2017).

Our approach to handling irregularities and variations in the input images is to use a bilateral filter followed by an adaptive threshold. An example of an input image of a standard pressure gauge can be seen in Figure 3 (a).

The output of running a bilateral filter on an image of a gauge can be seen in Figure 3 (b). The bilateral filter minimizes noise such as glass transition irregularities and trapped air pockets, which are common in pressure gauges.

A Gaussian mean adaptive threshold is used to binarize the filtered image as it is robust against variations in lighting conditions. The thresholded image can be seen in Figure 3 (c).

After the image has been binarized it is processed by the grassfire algorithm in order to label the objects.
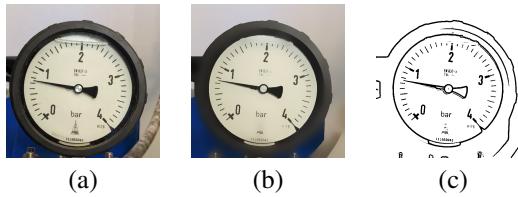
Figure 3: (a) The input image of a standard pressure gauge. (b) The bilateral filtered image. (c) The filtered image after being thresholded.

4.2 Circle Fitting

One of the most common methods to locate the gauge bezel is to use the Hough circle transform. However, this method has been found to perform poorly on gauges with chromed bezels, as they are highly reflective, which make the segmentation difficult and may result in only a part of the bezel being binarized. Therefore, a more error tolerant method inspired by (Gellaboina et al., 2013) is used as it has been found to provide more stable results on segmented circles.

4.2.1 The Circle Fitting Algorithm

In order to determine whether a given object in the binarized image is circular, the center is first determined by finding the centroid of the object via the image Moment of the object contours. Then an overlap value, V, is introduced as

$$V = \sum_{n=0}^{36} C \text{ AND } rot(C_r, 10 - n) \tag{1}$$

where C is the original object and C_r is a copy of the object, which is rotated 360 degrees around the center of C in steps of 10 degrees.

It is assumed that the gauge bezel object is always circular and among the largest objects, which means that it will stand out by accumulating the highest value V.

After having identified the most likely gauge bezel object, it is necessary to identify the circle described by this object as this information is crucial for recognizing the scale marks and the pointer. This is done by fitting a circle to the object using least squares circle fitting (Crawford, 1983).

Given a set of N input points $\{(x_i, y_i) | 0 < i \leq N\}$ each coordinate (x_i, y_i) is translated into another coordinate set (α_i, β_i) by

$$\alpha_i = x_i \circ \bar{x} \qquad \beta_i = y_i \circ \bar{y} \tag{2}$$

where the sample mean of the set of coordinates $(\bar{x}, \bar{y})$ is given by

$$\bar{x} = \frac{1}{N} \sum_i x_i \qquad \bar{y} = \frac{1}{N} \sum_i y_i \tag{3}$$

The least square center (α_c, β_c) is found by solving the system

$$\begin{bmatrix} M_{\alpha\alpha} & M_{\alpha\beta} \\ M_{\alpha\beta} & M_{\beta\beta} \end{bmatrix} \begin{bmatrix} \alpha_c \\ \beta_c \end{bmatrix} = \begin{bmatrix} \frac{1}{2}(M_{\alpha\alpha\alpha} \equiv M_{\alpha\beta\beta}) \\ \frac{1}{2}(M_{\beta\beta\beta} \equiv M_{\alpha\alpha\beta}) \end{bmatrix} \tag{4}$$

where $M_{\alpha\alpha} := \sum_i \alpha_i^2$, $M_{\alpha\beta} := \sum_i \alpha_i \beta_i$ and so forth. The center point can then be transformed back into the original coordinate system by letting $(x_c, y_c) = (\alpha_c, \beta_c) \equiv (\bar{x}, \bar{y})$ and the circle radius can be determined by

$$R = \sqrt{\alpha_c^2 \equiv \beta_c^2 \equiv \frac{M_{\alpha\alpha} \equiv M_{\beta\beta}}{N}} \tag{5}$$

With the gauge circle detected, characteristics of objects inside of the circle can now be determined.

4.3 Recognition of Scale Marks and Pointer

The idea of recognizing parts in the gauge dial originates from (Yi et al., 2017), who recognizes the scale marks on the dial using features of binary objects and the clustering technique K-means. This idea can be expanded by using parametric distributions to recognize both the scale marks and the pointer.

To describe the objects in the dial, five features are proposed, which will be outlined in this section along with sample distribution graphs that illustrate their capabilities to separate the objects.

The rotated bounding box ratio is a feature meant to capture the oblongness of an object. Each object is rotated to be aligned with the horizontal axis before the bounding box ratio is calculated.

The mass of an object is simply the number of pixels it contains. To make sure that the mass does not reach unnecessarily large values, it is transformed with the natural logarithm.

The compactness is the mass related to the area of the bounding box.

The distance to gauge center is the Euclidean distance between the object's bounding box center and the center point of the gauge bezel. To ensure that values are independent to the gauge size in the frame, the distance is normalized by the gauge radius.

The orientation inaccuracy is given by the Euclidean distance of the orthogonal vector between the orientation vector of a given object and the gauge center. The eigenvector of the largest eigenvalue found using PCA defines the orientation vector. The distance is normalized by the gauge radius.

By describing objects according to these simple features it becomes possible to differentiate between them. As illustrated in Figure 4, the pairwise combinations of the proposed features reveal structures that

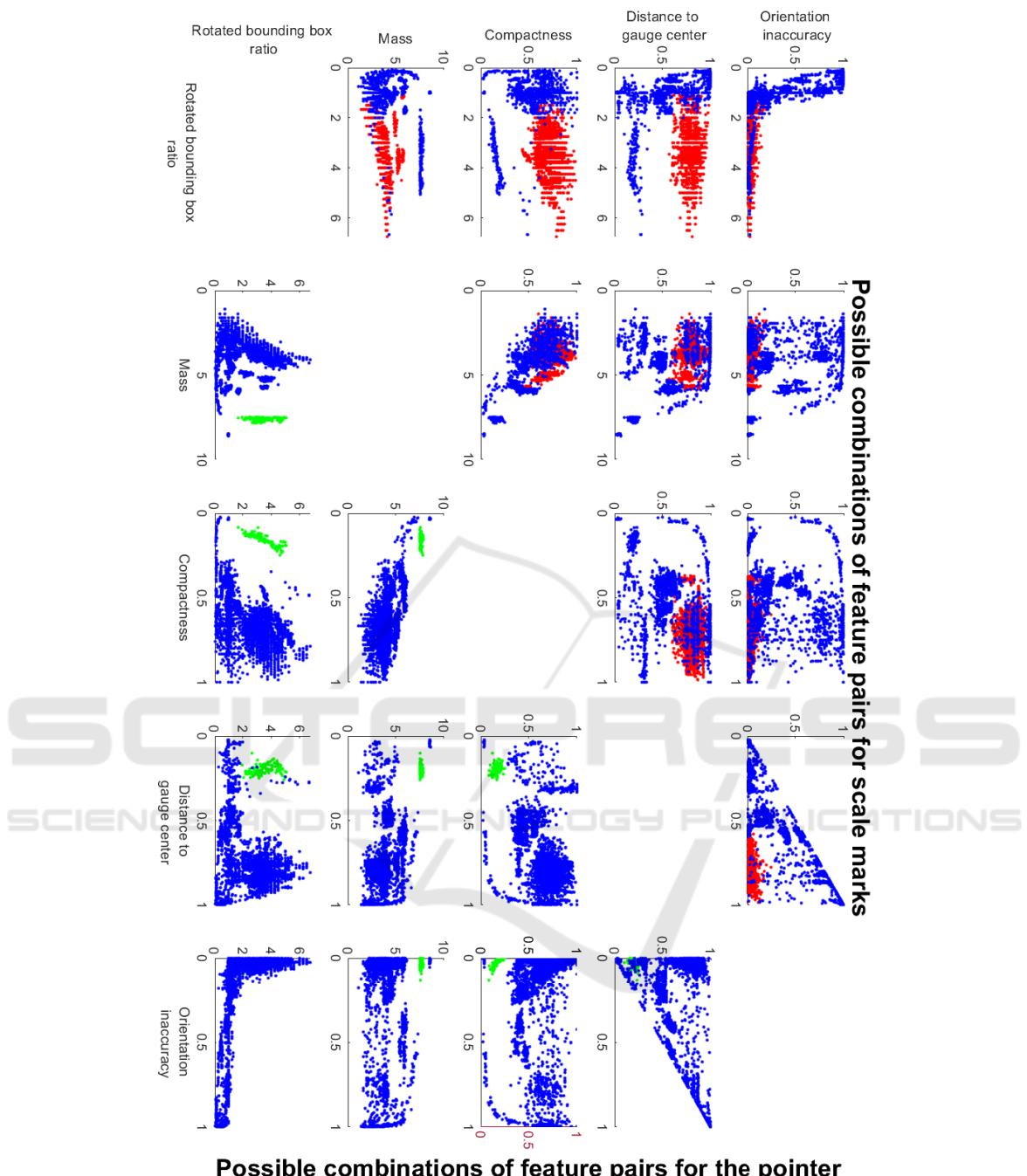**Possible combinations of feature pairs for the pointer**

Figure 4: Graphs showing all the feature-pairs and their ability to separate objects. The graphs on the left and right side of the empty diagonal shows the same feature-pairs but with a different focus. On the left, the red dots illustrate the scale marks and the blue dots represent noise, which include the pointer objects. On the right, the green dots illustrate the pointer object and the blue is noise, which include the scale marks.

are capable of separating the objects. All the graphs are based on manually classified objects in 49 images from each of three training videos of pressure gauges that are presented later.

One example is the feature space spanned by mass and distance to gauge center, which clearly separa-

tes the pointer object from everything else. Another example is the distance to gauge center and rotated bounding box ratio, which separates scale marks and noise.

The samples give rise to the assumption that objects in the dial can be classified using multivariate

Gaussian distributions. In most of the presented examples a single Gaussian distribution should be adequate to describe the relevant object, whereas two distributions seem to be needed in order to cover the noise.

The Gaussian multivariate distributions are described by a mean vector, μ_k, and covariance matrix Σ_k, where the subscript, k, denotes the given distribution. A mixing coefficient α_k is introduced to ensure that the probability density function integrates to 1 (Bishop and Nasrabadi, 2007). An object can then be described by its feature vector, $\mathbf{x}$, and the likelihood of that object belonging to a class, i, can be expressed by

$$\mathcal{L}(i|\mathbf{x}) = \left\{ \sum_{k \in i} \alpha_k \mathcal{N}(\mathbf{x}|\mu_k, \Sigma_k) \right. \tag{6}$$

Parameters are fitted using unlabelled samples from the training videos, which are described later, and the unsupervised learning technique Expectation Maximization (EM). The algorithm is run until convergence using initial mean vectors, and diagonal covariance matrices based on the manually classified objects. Two feature-pairs are found to be able to distinguish scale marks, the pointer and noise from each other.

The feature-pair consisting of the distance to gauge center and rotated bounding box ratio is used to classify scale marks. A visualization of the distributions before and after EM can be seen in Figure 5. The classification of new objects is based on the likelihood of the objects belonging to a given class.

The mass and distance to gauge center is used to classify the pointer object and a presentation of the distribution before and after EM is shown in Figure 5. When classifying the pointer, only one object needs to be found. Hence all objects are sorted by their Mahalanobis distance to the pointer distribution and the closest object is assumed to be the pointer.

4.4 Estimation of the Pointer Angle

The angle of the pointer is found using principal component analysis (PCA), which is defined as an orthogonal projection of the data set onto a subspace that maximizes the variance of the projected data.

The binary pixels of the pointer object can be interpreted as a set of two-dimensional points, $\mathbf{x}$, and by projecting $\mathbf{x}$ onto the one-dimensional subspace u_1, that maximizes the variance of the set, the direction of the pointer can be determined.

The mean of the projected data can be described as $u_1^T \bar{\mathbf{x}}$, where $\bar{\mathbf{x}}$ is the mean of $\mathbf{x}$. The variance of the
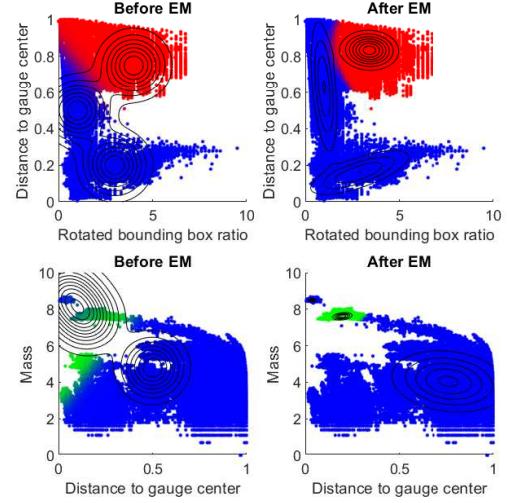

Figure 5: Visualization of distributions before and after estimating parameters using the EM algorithm.

projected data can then be found by

$$u_1^T S u_1 = \frac{1}{N} \left\{ \sum_{n=1}^{N} \left\{ u_1^T \mathbf{x}_n \circ u_1^T \bar{\mathbf{x}} \right\} \right. \tag{7}$$

where N is the amount of points in $\mathbf{x}$ and the covariance matrix, S, is given by

$$S = \frac{1}{N} \left\{ \sum_{n=1}^{N} \left(\mathbf{x}_n \circ \bar{\mathbf{x}} \right) \left(\mathbf{x}_n \circ \bar{\mathbf{x}} \right)^T \right. \tag{8}$$

A practical solution to maximizing the projected variance, $u_1^T S u_1$, is to set u_1 equal to the eigenvector of the largest eigenvalue found in the covariance matrix (Bishop and Nasrabadi, 2007).

However, the orientation of the object needs to be determined as the vector can point in two directions seen from the object's perspective. The pointy end of the pointer is assumed to always be longer than the blunt end relative to the center. Therefore, the direction vector formed from the center of the gauge to the bounding box center of the pointer object is used to determine the orientation.

With this known, the pointer vector with the lowest angle to the direction vector can be determined using the angle between the vectors. To improve the direction vector obtained by PCA, the object is cropped with a circle that has the same center as the gauge and a radius of one fifth of the radius of the gauge bezel. This is done because the pointer occasionally passes over the gauge numbers which produces noise at the tip of the pointer.

The resulting method will extract the angle in each frame of the video. This angle will have to be related to a reference location to obtain an absolute angle as

seen in Figure 6, resulting in a time series expressing the pointer's angle as a function of time.
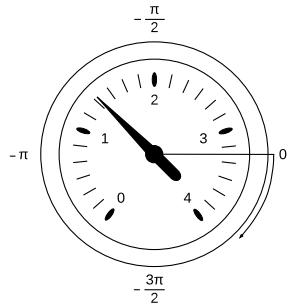

Figure 6: Visualization of how the rotation of the pointer is referenced.

4.5 Data Time Series

As the angle of the pointer can be identified its transient behaviour throughout a video can now be considered. Without any filtering, the pressure time series becomes noisy as seen in Figure 7. The noise is comprised of misinterpreted pointer angles and scenarios where a direction could not be determined.

Pressure time series recorded manually with digital pressure sensors from waste water pumping stations were obtained by consulting [*an anonymous engineering company*], which specializes in waste water systems. An FFT of the received time series showed that the important frequency components were below 1Hz. Therefore, based on the Nyquist–Shannon sampling theorem the frequency resolution should be satisfactory at a minimum of 2 Hz.

To remove outliers, the 30 Hz recorded signal is filtered by a tenth-order low pass FIR filter, which has a cutoff frequency of 2 Hz. An example of a recorded time series before and after being filtered is presented in Figure 7.
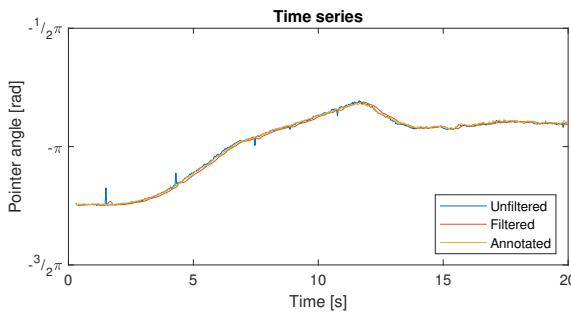

Figure 7: Graph illustrating a raw and noisy signal in blue and its low pass filtered counterpart in red.

5 DATA SET

Figure 8: Images from the *train1, train2* and *train3* recordings, seen from left to right, respectively.

The data set that has been used consists of 3 training videos and 7 testing videos of running analog pressure gauges used in the waste water industry. The recordings have been edited to mainly contain the gauge bezel and scaled to a size of $512 \subseteq 512$ pixels. However, the raw videos and additional recorded videos are also provided in the published data set.

The 3 training videos are recorded under a variety of conditions to diversify the training set. *train1* is stationary with bright lighting, *train2* is stationary with ambient lighting and *train3* is hand held with ambient lighting. Images from the three recordings can be seen in Figure 8.

The 7 testing videos are edited to match the format of the training videos and are provided along with their corresponding annotations. They are named *test1, test2, ..., test7* and are all recorded with a stationary camera under ambient lighting but each has a unique combination of characteristics, such as shaking, erratic pointer, angle, water level, bezel reflection and light glare that make them relevant to test against. Images from the seven recordings can be seen in Figure 9.

6 RESULTS

Figure 12 shows the results of running the algorithm on *test1*. The grey dashed lines in the figure corresponds to a recognized mark in the first frame of the video. The algorithm recognizes scale marks in all frames, but for visual purposes, only scale marks from the first frame are used. Comparing each measurement of the pointer's angle to the annotated truth, an error is assigned.

The histogram plot presented in Figure 10 illustrates the absolute error between the annotated and measured signal in radians. The error is normally distributed with a mean and standard deviation of 0.02 and 0.02 radians, respectively. This low error corresponds to the pointer being approximately 1 degree offset according to the annotated data and in a few cases 2-3 degrees off. The observable negative tail in the negative area may by caused by periods in *test1* where the

Figure 9: Images from the *test1, test2, ..., test7* recordings, seen from left to right, respectively.

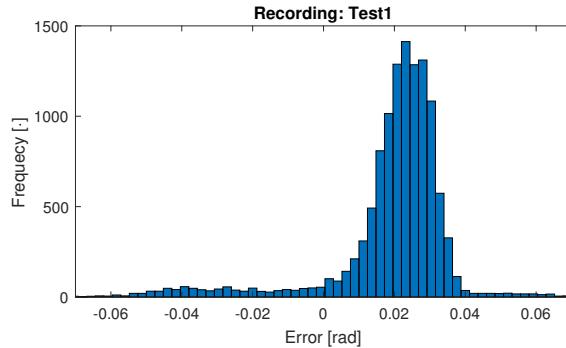Figure 10: Histogram of the absolute error between the annotated and measured signal of the captured time series of *test1*.
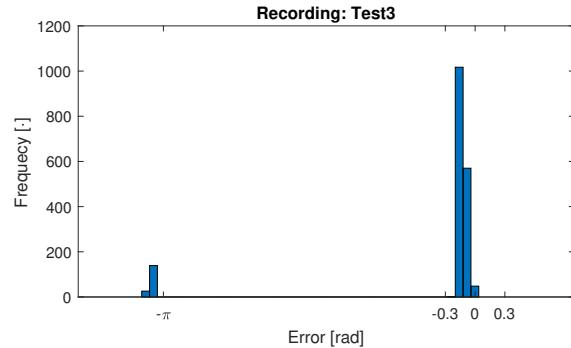

Figure 11: Histogram of the absolute error between the annotated and measured signal. Notice how there is a significant accumulation of erroneous measurements around $\circ\pi$.

pointer is covered or by a periodically present shadow from the pointer.

In some frames, the implementation of the algorithm fails to produce a meaningful angle of the pointer, at which it gives up and stores NAN as the result. This is illustrated in Figure 13 that shows the computed signal from *test2* with almost no detected pointer angles in the last part of the signal.

Figure 14 shows the results of running the proposed algorithm on *test3*. Here it should be noticed how the computed angle fluctuates heavily. By inspection of the annotated data, it can be seen that the pointer does not change as much as predicted during the given time periods.

However, as emphasized by Figure 11 a significant error occurs at almost exactly $\circ\pi$, which is analogue for a half circle rotation. By inspection of the recorded video it can be seen that the pointer is erratic, and in some frames the pointy end is nearly invisible due to heavy motion blur. In those frames the algorithm misjudges the direction of the pointer to be the blunt end resulting in an error of $\circ\pi$ radians.

Table 2 shows the number of hits and misses as well as the mean and standard deviation of the pointer angle error in radians for the seven test videos. Hits describe the number of frames where the gauge bezel, pointer and marks are found such that the angle of the pointer can be estimated. Misses describe the opposite, where the system is not capable of determining an angle of the pointer relative to the bezel.

Inspection of *test2* and *test6* shows that the low hit rate is due to varying lighting conditions, which is es-

pecially apparent in the chrome gauge bezels making them undetectable for the system in large parts of the recordings.

6.1 Comparison with State-of-the-Art

Over the last couple of decades, many articles have been published on how to digitise analogue dials using computer vision and a comparison between the state-of-the-art methods would, therefore, be appropriate. However, even though the meticulousness of the publications vary, they share the same bad traits which makes such a comparison difficult to realise.

As presented in the first row of Table 1, the data that have been used for testing the methods generally consists of images of a single dial, with the exception of (Jiannan Chi, 2015) and (Yang et al., 2014). Furthermore, the results are in many cases based on only a few images taken from the same angle and light condition (Ye et al., 2013)(Yi et al., 2017)(Sun et al., 2014)(Jiale et al., 2011)(Wang et al., 2013). This means that, even though the results may be good, there is a high possibility that the methods have been overfitted to their respective setups. Lastly, none of the authors has published their source code or test data, so it is not possible to replicate their findings.

In order to create a foundation for future benchmarking tests and comparisons, the entire source code used for the presented work is published along with the raw and edited test and training videos.
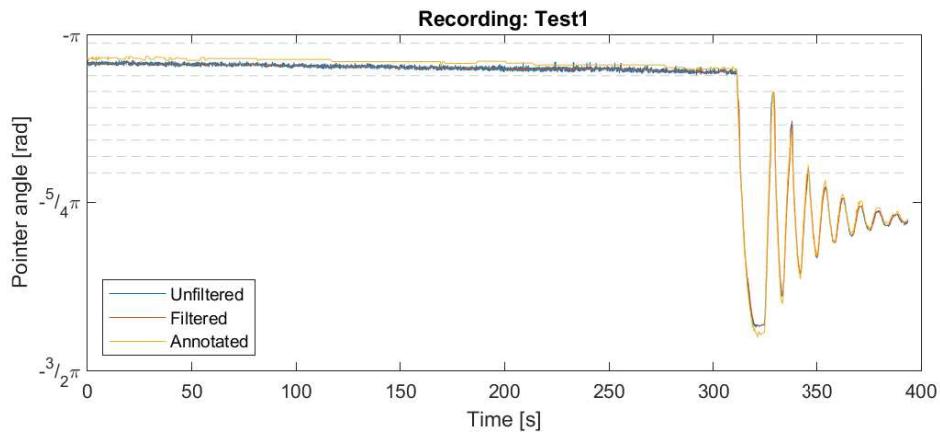
Figure 12: Time series captured by processing *test1* using the proposed method. Notice how the measured pointer angle is closely related to the annotated angle throughout the recording.
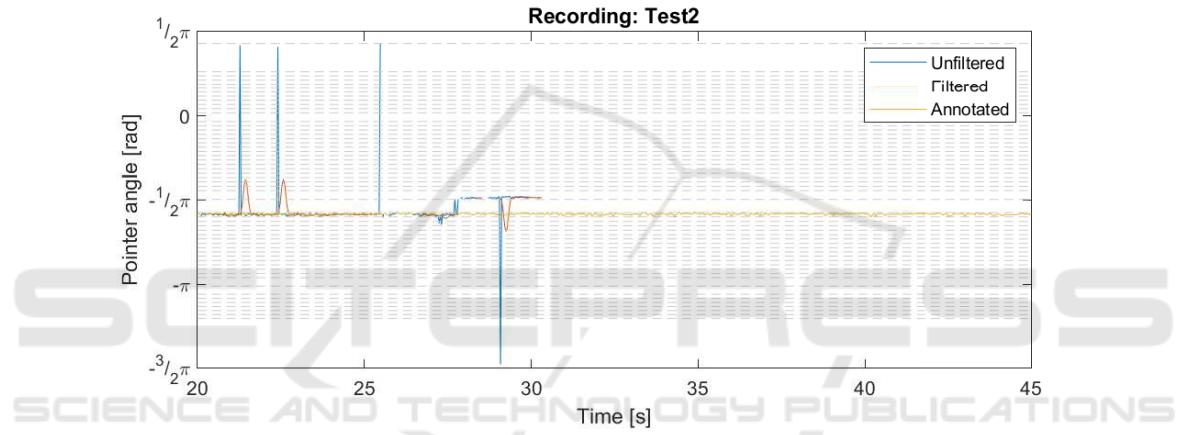

Figure 13: Results from performing the algorithm on *test2*. The system fails to produce any meaningful angle of the pointer in a significant amount of frames.
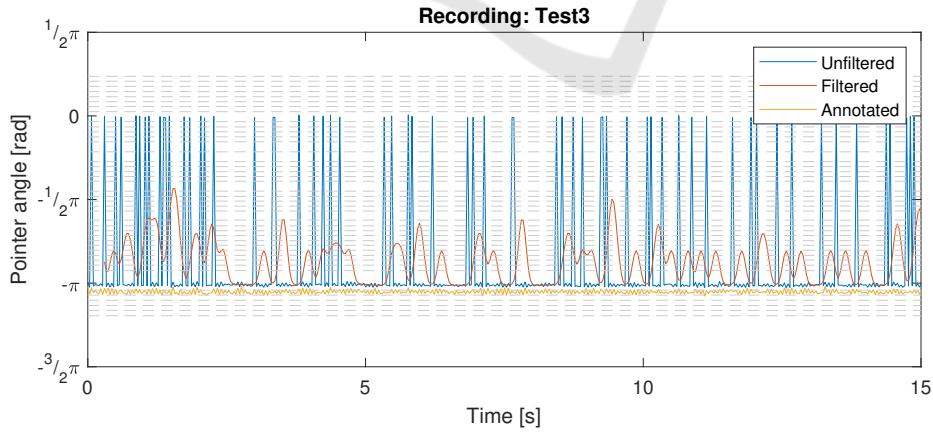

Figure 14: Results from performing the algorithm on *test3*. The measured signal jumps incorrectly from ∘π to 0 often. This is due to motion blur of the pointer in *test3*.

Table 1: Overview of state-of-the-art methods with regards to accessibility and the number of dials involved in the work.

	J. Chi	*X. Ye*	*C. Zheng*	*M. Yi*	*B. Sun*	*H. Jiale*	*B. Yang*	*Q. Wang*	Proposed
No. of Dials	2	1	1	1	1	1	8	1	10
Open Source	No	No	No	No	No	No	No	No	Yes
Public Data	No	No	No	No	No	No	No	No	Yes

Table 2: Classification and error rate of the proposed method when processing the seven test videos.

	Hit	Miss	μ [rad]	σ [rad]
test1	11811	0	0.02	0.02
test2	967	1253	-0.47	1.28
test3	1801	0	-0.42	0.39
test4	1111	0	0.08	0.32
test5	451	0	-0.12	0.39
test6	347	704	-6.07	0.56
test7	571	2	-0.13	0.61

7 CONCLUSION

A method to automatically digitize analog circular gauges using computer vision is presented with an application example of a video recording of a pressure gauge translated into a digital time series.

The method is based on segmenting objects in each frame using Gaussian adaptive mean thresholding and subsequently classifying the objects using probability distributions estimated with the unsupervised learning method Expectation Maximization. The output of the algorithm is an estimated angle of the pointer object, which is determined using PCA.

Recordings of seven pressure gauges, mounted on waste water pumping stations, have been processed by the algorithm. The mean and standard deviation of the angle error are calculated for each of the videos with the best case of μ = 0.02 radians and σ = 0.02 radians.

However, in three of the recordings, significant errors are present. In *test2* and *test6* the bezel is made from a reflective material, which makes it difficult to segment objects properly with the proposed method due to reflections. In another case, a problem is identified where the angle of the pointer is miscalculated by $\circ\pi$ radians due to motion blur.

The shortcomings that have been uncovered in the tests are related to specific scenarios, which should be taken into consideration during the next iteration of the project. Generally, the results are very promising and there is a great potential in the proposed parametric classification method.

The source code is published at (Lauridsen and Grassmé, 2018a) and the test and training data is published at (Lauridsen and Grassmé, 2018b).

8 FUTURE WORK

The current system only processes a single frame at a time, neglecting the benefits that might arise from utilizing data from neighbouring frames. As an example, to achieve better estimates for the circle, center or for more accurate scale creation the temporal neighboring data could be utilized. This could also be used to reduce the errors introduced by motion blur, where the angle is incorrectly determined by the blunt end of the pointer.

Exploring other features, higher feature spaces or other compositions could possibly increase the accuracy and make the proposed solution more robust. The training data could also be more diverse in order to better generalize to different types of dials. Lastly, the level of automation can be improved by recognizing the dial numbers and associating those numbers to the scale marks.

REFERENCES

Alegria, F. C. and Serra, A. C. (2000). Computer vision applied to the automatic calibration of measuring instruments. *Measurement*, 28(3):185 – 195.

Bishop, C. M. and Nasrabadi, N. M. (2007). Pattern Recognition and Machine Learning. *Journal of Electronic Imaging*, 16(4):049901.

Crawford, J. (1983). A non-iterative method for fitting circular arcs to measured points. *Nuclear Instruments and Methods in Physics Research*, 211(1):223–225.

Gellaboina, M. K., Swaminathan, G., and Venkoparao, V. (2013). Analog dial gauge reader for handheld devices. In *2013 IEEE 8th Conference on Industrial Electronics and Applications (ICIEA)*. IEEE.

Jiale, H., En, L., Bingjie, T., and Ming, L. (2011). Reading recognition method of analog measuring instruments based on improved hough transform. In *IEEE 2011 10th International Conference on Electronic Measurement Instruments*, volume 3, pages 337–340.

Jiannan Chi, Lei Liu, J. L. Z. J. G. Z. (2015). Machine vision based automatic detection method of indicating values of a pointer gauge. In *Mathematical Problems in Engineering, Article ID 283629*, volume 2015.

Lauridsen, J. S. and Grassmé, J. G. (2018a). Bitbucket pressure gauge reader source code. https://bitbucket.org/aauvap/pressure-gauge-reader [Link].

Lauridsen, J. S. and Grassmé, J. G. (2018b). Kaggle pressure gauge reader data set. http://kaggle.com/juliusgrassme/pressure-gauge-reader-data [Link].

Sablatnig, R. and Kropatsch, W. G. (1994). Automatic reading of analog display instruments. In *Proceedings of 12th International Conference on Pattern Recognition*, volume 1, pages 794–797 vol.1.

Selvathai, T., S, J. S., Ramesh, S., and KK, R. (2017). Automatic interpretation of analog dials in driver's instrumentation panel. In *2017 Third International Conference on Advances in Electrical, Electronics, Information, Communication and Bio-Informatics (AEEICB)*. IEEE.

Sun, B., Zhang, C., Liu, Z., Qian, B., and Zhang, H. (2014). Study of fpga-based visual detection for pointer dial. In *The 26th Chinese Control and Decision Conference (2014 CCDC)*, pages 1467–1472.

Wang, Q., Fang, Y., Wang, W., Wu, M., Wang, R., and Fang, Y. (2013). Research on automatic reading recognition of index instruments based on computer vision. In *Proceedings of 2013 3rd International Conference on Computer Science and Network Technology*, pages 10–13.

Yang, B., Lin, G., and Zhang, W. (2014). Auto-recognition method for pointer-type meter based on binocular vision. *JCP*, 9(4):787–793.

Ye, X., Xie, D., and Tao, S. (2013). Automatic value identification of pointer-type pressure gauge based on machine vision. *JCP*, 8:1309–1314.

Yi, M., Yang, Z., Guo, F., and Liu, J. (2017). A clustering-based algorithm for automatic detection of automobile dashboard. In *IECON 2017 - 43rd Annual Conference of the IEEE Industrial Electronics Society*, pages 3259–3264.

Zheng, C., Wang, S., Zhang, Y., Zhang, P., and Zhao, Y. (2016). A robust and automatic recognition system of analog instruments in power system by using computer vision. *Measurement*, 92:413 – 420.